ЖЭТФ, 2014, том 145, вып. 1, стр. 77–83

APPLYING AN IMPROVED PHONON CONFINEMENT MODEL TO THE ANALYSIS OF RAMAN SPECTRA OF GERMANIUM NANOCRYSTALS

V. A. Volodin [a,b*], ***D. V. Marin*** [a,b], ***V. A. Sachkov*** [c], ***E. B. Gorokhov*** [a], ***H. Rinnert*** [d], ***M. Vergnat*** [d]

[a] *Rzhanov Institute of Semiconductor Physics, Siberian Branch, Russian Academy of Sciences 630090, Novosibirsk, Russia*

[b] *Novosibirsk State University 630090, Novosibirsk, Russia*

[c] *Omsk Scientific Center, Siberian Branch, Russian Academy of Sciences 644040, Omsk, Russia*

[d] *Institut Jean Lamour UMR CNRS 7198 — Université de Lorraine, B.P. 70239 54506, Vandœuvre-lès-Nancy Cedex, France*

Received April 20, 2013

The improved phonon confinement model developed previously [11] is applied for definition of germanium nanocrystal sizes from the analysis of its Raman scattering spectra. The calculations based on the model allow determining the sizes of germanium nanocrystals more precisely from the analysis of their Raman spectra. In some cases, the comparative analysis of Raman data and electron microscopy data is carried out, and good agreement is observed.

DOI: 10.7868/S0044451014010076

1. INTRODUCTION

Semiconductor nanocrystals (NCs) in dielectric films have attracted the interest of researchers because of their electrical and optical properties tunable by altering the size and also because of their potential in new optoelectronic and nonvolatile memory devices. Due to electron confinement, the optical gap of semiconductor NCs is size-dependent [1, 2], which is usually called quantum size effect. A semiconductor NC embedded in a wide-gap insulating matrix has a discrete electron spectrum due to localization of the electron wave function in three directions [3]. In germanium NCs, the quantum size effect should be stronger due to a larger exciton Bohr radius in Ge compared with Si. The vibrational spectra of quantum dots also differ from the vibrational spectra of bulk materials, and they are determined by the composition, size, shape, and mechanical stresses of the quantum dots. For this reason, analysis of the vibrational spectrum of nanostructures based on Raman spectroscopy is widely used for studying the quantum dots and can give information about their structure (size and shape).

Si NCs are studied more intensively than Ge NCs. For example, more than thirty years ago, it was experimentally observed that Raman spectra of polycrystalline Si and bulk Si are different [4]. The polycrystalline Si studied in [4] contains Si NCs, and the authors explained the shift and broadening of optical phonon Raman peaks by softening of the conservation law of the quasimomentum of phonons due to phonon confinement in NCs. The quasimomentum conservation law is softened according to the Heisenberg uncertainty principle. The phonon confinement model (PCM) proposed in [4] was developed and generalized in [5], where it was also applied to one dimensional objects (quantum well wires). In [5], the dependence of the calculated Raman spectra on phonon weight functions was first discussed. Because of its clear physical approach, the

*E-mail: volodin@isp.nsc.ru

PCM is being developed up to now [6–11]. The model was considerably improved for Si NCs by taking the angle dispersion of transverse and longitudinal phonons into account [11]. The phonon dispersion was calculated with the Keating model instead of being approximated by empirical expressions, as was done in earlier approaches. The PCM was also applied to the analysis of sizes of Ge NCs [12–18], but the above-mentioned factors were not taken into account. The present work is devoted to applying the improved PCM to Ge NCs and to comparative analysis of calculated and experimental Raman spectra.

2. EXPERIMENTAL

In this study, the correctness of the model is verified by comparative analysis of the calculated and experimental Raman spectra. The triple Raman spectrometer T64000 (Horiba Jobin Yvon) with micro-Raman setup was used. All experimental spectra were recorded in the backscattering geometry at room temperature using the 514.5-nm line of an Ar^+ laser. The incident light was polarized linearly, the polarization of scattered light was not analyzed. The spectral resolution was not worse than 1.5 cm^{-1}. The detector was a silicon-based CCD matrix, cooled with liquid nitrogen. The power of the laser beam reaching the sample was 2 mW. To avoid heating by the laser beam, the sample was placed slightly farther than the focus, and the spot size was about 30 μm.

Films containing Ge NCs were obtained using two methods. The first is deposition on a cooled substrate from supersaturated germanium monoxide (GeO) vapor. The GeO is metastable in the solid phase and dissociates at the temperature about 300 °C (solid-state chemical reaction):

$$2\mathrm{GeO(solid)} \rightarrow \mathrm{Ge(solid)}+\mathrm{GeO_2(solid)}. \qquad (1)$$

Depending on the substrate temperature, undissociated GeO films or Ge:GeO_2 films with different sizes of Ge clusters can be deposited. Using post-deposition thermal annealing treatments at different temperatures, Ge clusters can be crystallized to obtain Ge NCs of different sizes. The higher the annealing temperature is, the bigger the Ge NCs are. The first method is described in more detail elsewhere [15, 19]. If the deposition of GeO occurs at higher temperatures, the solid-state chemical reaction also takes place, but in this case the Ge NCs are formed, and post-growth annealing is not needed. According to the electron microscopy data, the sizes of Ge NCs can range from 2.5 nm (growth at 450 °C) to 7–8 nm (growth at 580 °C).

The second method is successive evaporation of GeO_2 and SiO_2 by an electron beam in high vacuum (about 10^{-8} Torr) and deposition onto substrates maintained at 100 °C. The pressure during the evaporation increases to 3×10^{-6} Torr due to the partial decomposition of GeO_2. The deposition rate of 0.1 nm/s was controlled by a quartz microbalance. In fact, under electron bombardment of GeO_2, its partial decomposition into Ge, O_2 and GeO occurs. The last two components are more volatile, but, unlike O_2, GeO is easily deposited onto a cool substrate. Hence, the deposited germanium oxide is substoichiometric, namely GeO_x, where x is close to 1 [20]. In the same paper [20], it was also shown that silicon oxide layers have a composition very close to SiO_2. Three multilayer structures containing 10 periods of GeO_x(4 nm)/SiO_2(4 nm), GeO_x(2 nm)/SiO_2(4 nm), and GeO_x(1 nm)/SiO_2(4 nm) were covered by a SiO_2 cap layer with a thickness equal to 100 nm. The samples were annealed in high-vacuum quartz tube with a tubular oven. The heating rate was 10 °C/min. When the annealing temperature (600 °C) was reached, the samples were held in the oven for 30 min, then the oven was removed and the films cooled naturally. The second method is described in more detail elsewhere [21, 22].

3. RESULTS AND DISCUSSION

3.1. Improved PCM and Raman spectra for Ge NCs

As mentioned above, the PCM allows calculating the Raman spectra for NCs of various sizes [9–11]. The PCM was considerably improved by taking dispersion of phonons into account not only in the magnitude of the quasimomentum but also in its direction [11]. A significant refinement of the model was reached by using the widely approved Keating model to calculate the phonon dispersion instead of approximating it by empirical expressions as was done in earlier approaches [11]. In general, for crystals with a diamond-type lattice (like Si and Ge), there are six phonon branches with dispersions $\omega_i'(q)$.

The phonon dispersions of Ge and Si are similar, and hence the first-order Raman spectrum for the phonon weight function $W(\mathbf{r}, L) = \exp(-4r^2/L^2)$ is [11]

$$I(\omega) \approx \sum_{i=1}^{6} \int_{0}^{q_{max}} \exp\left(-\frac{q^2 L^2}{8}\right) \times$$

$$\times \frac{[n(\omega_i'(q))+1]\, q^2 dq}{\omega_i'(q)\left[\left(\omega-\omega_i'(q)\right)^2+(\Gamma/2)^2\right]}, \quad (2)$$

where L is the diameter of NCs,

$$n\left(\omega'(q)\right) = \left[\exp\left(\frac{\hbar\omega'(q)}{kT}\right)-1\right]^{-1}$$

is the Bose–Einstein factor, and Γ is the full width at half maximum of the Raman peak of a single phonon. Wavenumbers q range from 0 to q_{max} (an edge of the Brillouin zone). We note that for directions with high symmetry ($\langle 100\rangle$ and $\langle 111\rangle$), some phonon branches are degenerate. The density of states for phonons is proportional to $q^2 dq$.

In some approaches, the phonon frequencies are determined using quantum mechanical calculations from first principles [23, 24], but this method requires large computational resources, while NCs with diameters more than 5 nm contain more than one thousand atoms. To calculate the phonon dispersion, the Keating model of valence forces [25] was therefore used, as in [11]. In this simple, but sufficiently adequate model, the elastic energy of the crystal depends on the bond length and on the deviation of the bond angle from ideal tetrahedral angles.

We consider interaction only between nearest-neighbor atoms. For a crystal with a diamond-type lattice, the elastic energy of the unit cell is

$$E = \frac{3}{16}\sum_i \sum_j \frac{k_l}{a^2}\left[(\mathbf{r}_i-\mathbf{r}_j)^2 - \frac{3a^2}{16}\right]^2 +$$

$$+\frac{3}{8}\sum_i \sum_{k,j>k}^{4} \frac{k_\varphi}{a^2}\left[(\mathbf{r}_i-\mathbf{r}_j)\cdot(\mathbf{r}_i-\mathbf{r}_k)+\frac{a^2}{16}\right]^2, \quad (3)$$

where k_l and k_φ are elastic constants (Hooke's coefficients) and a is the lattice constant. TO and LO phonons at the Brillouin zone center are degenerate for crystals with the diamond type lattice. The frequency is given by

$$\omega_\Gamma = \sqrt{\frac{8(k_l+3k_\varphi)}{3m}}, \quad (4)$$

where m is the mass of Ge atoms. For germanium, the frequencies of TO and LO phonons at the Brillouin zone center are equal to 301 cm^{-1}. Hence, the elastic constants k_φ and k_l are not independent (see formula (4)). The elastic constant k_l was determined from the approximation of calculated dispersions in directions $\langle 100\rangle$, $\langle 110\rangle$, and $\langle 111\rangle$ to experimental dispersions obtained from neutron scattering data [26].

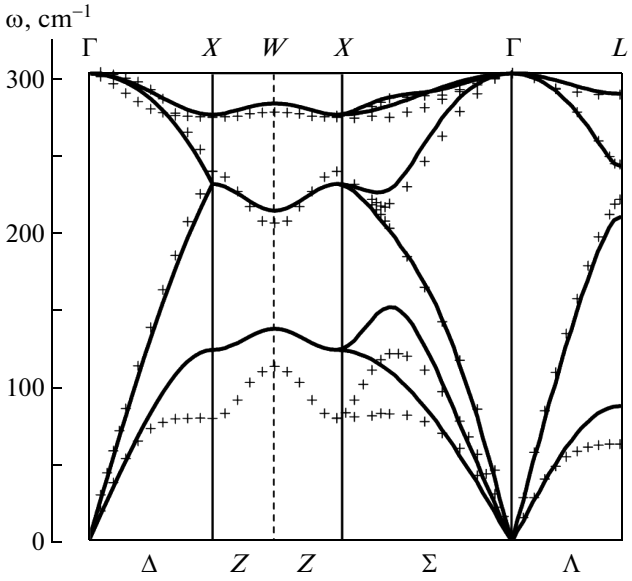

Fig. 1. Phonon dispersion for bulk germanium: experimental [26] (figures) and calculated (lines) using the Keating model

It is important to consider phonons of different directions, because in experiment, Raman signal comes from a large number of randomly oriented NCs, and all phonon modes are intermixed. The exact expressions for phonon dispersions in directions $\langle 100\rangle$, $\langle 110\rangle$, and $\langle 111\rangle$ for the Keating model are published in [11] and are very cumbersome. But because the energy of three-particle interaction is much lower than the energy of two-particle interaction, $k_\varphi \ll k_l$, the best approximation of the calculated dispersion to experimental ones (Fig. 1) is achieved if the ratio k_φ to k_l is equal to $8\cdot 10^{-2}$. We note that as we calculate Raman spectra for optical phonons, the approximation of optical branches was implemented with higher accuracy than for acoustical branches. The frequencies of TO and LO phonons at the center of the Brillouin zone (ω_Γ) are known with higher accuracy than the frequencies of phonons at others points of the Brillouin zone. We therefore assume that the frequency of long-wave optical phonons must exactly match ω_Γ. The Taylor series expansion for the phonon dispersion (using the parameter $k_\varphi/m\omega_\Gamma^2$) rapidly converges. In what follows, we therefore use the approximate expression only with the linear term in the parameter $k_\varphi/m\omega_\Gamma^2 = 3.8\cdot 10^{-2}$.

For the ⟨100⟩ direction, the frequencies of LO and TO phonons depend on the wavenumber q as

$$\omega_{LO}(q,0,0) = \omega_\Gamma \left|\cos\frac{\pi q}{4}\right| \left(1 + 8\frac{k_\varphi}{m\omega_\Gamma^2}\sin^2\frac{\pi q}{4}\right),$$
$$\omega_{TO}(q,0,0) = \omega_\Gamma \left[1 + 2\frac{k_\varphi}{m\omega_\Gamma^2}\left(\cos(\pi q) - 1\right)\right]. \quad (5)$$

For the ⟨110⟩ direction, one of the TO phonons is exactly transverse, but two optical phonon branches with low symmetry are intermixed, and marked as O_1 and O_2. For the ⟨110⟩ direction, the frequencies of optical phonons depend on the wavenumber q as

$$\omega_{O_1}(q,q,0) = \omega_\Gamma \left[1 + \frac{k_\varphi}{m\omega_\Gamma^2} \times \right.$$
$$\left. \times \frac{3\cos(\pi q) + \cos(2\pi q) + \cos(3\pi q) - 5}{\cos(\pi q) + 3}\right],$$
$$\omega_{O_2}(q,q,0) = \omega_\Gamma \left[\frac{1}{2}\sqrt{\cos(\pi q) + 3} - \frac{k_\varphi}{m\omega_\Gamma^2} \times \right. \quad (6)$$
$$\left. \times \frac{4\sin(\pi q/2)\left[9\cos(\pi q) + 7\right]}{\left[\cos(\pi q) + 3\right]^{3/2}}\right],$$
$$\omega_{TO}(q,q,0) = \omega_\Gamma \left[1 - 4\frac{k_\varphi}{m\omega_\Gamma^2}\sin^2\left(\frac{\pi q}{2}\right)\right].$$

For the ⟨111⟩ direction, the frequencies of LO and TO phonons depend on the wavenumber q as

$$\omega_{LO}(q,q,q) = \omega_\Gamma \sqrt{\sqrt{6\cos(2\pi q) + 10} + 4} \times$$
$$\times \left[\frac{\sqrt{2}}{4} + \frac{k_\varphi}{m\omega_\Gamma^2}\left(\frac{7\sqrt{2}}{3} - \frac{9\cos(2\pi q) + 47}{6\sqrt{3\cos(2\pi q) + 5}}\right)\right], \quad (7)$$
$$\omega_{TO}(q,q,q) = \omega_\Gamma \left[1 - 2\frac{k_\varphi}{m\omega_\Gamma^2}\sin^2(\pi q)\right].$$

In this approximation, the maximum relative error in comparison with the exact solution for the Keating model does not exceed 2.5 %.

To calculate the first-order Raman spectrum, we should use expressions (5)–(7) in formula (2). Dispersion in different directions should be used with its corresponding weight. There are six physically equivalent ⟨100⟩ directions, and hence the weight of this dispersion is six. Similarly, the weight of dispersion along the ⟨111⟩ and ⟨110⟩ directions is respectively equal to 8 and 12. Thus, all calculations were performed with the phonon dispersion in the Keating model, taking the phonon dispersion for the three main directions in germanium into account.

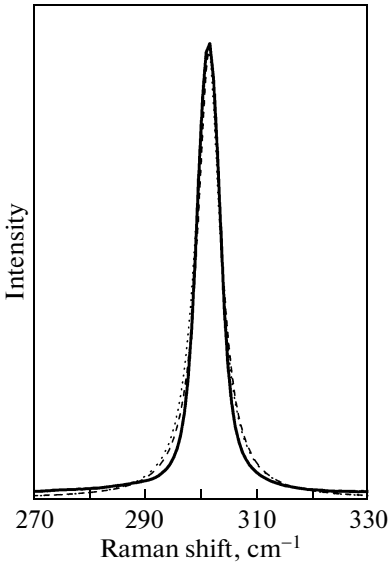

Fig. 2. Raman spectra: solid line is the experimental spectrum for bulk germanium; dashed and dotted lines are the calculated spectra for Ge NCs with the respective diameters 50 and 20 nm. The spectra are calculated using the PCM, phonon dispersion is calculated using the Keating model, and the angular dispersion of TO and LO phonons is taken into account

3.2. Calculation results in comparison with experiment

Figure 2 shows the calculated Raman spectra of NCs with the diameter 50 and 20 nm and the experimental Raman spectrum of the bulk germanium for comparison. All spectra were calculated within the improved PCM, formula (2) was used to calculate the Raman spectra, and formulas (5)–(7) were used to calculate the phonon dispersion. The spectra have been normalized. The calculated and experimental spectra are in good agreement. Because the position and width of the experimental spectrum of bulk germanium are close to the position and width of the calculated spectrum of Ge NC with the diameter 20 nm, we can conclude that the phonon correlation length (in other words, the size of the phonon wave packet) in bulk germanium is about 20 nm or a little shorter.

Figure 3 shows the results of calculations of the Raman spectra of germanium NCs of different diameters. It is seen that for the germanium NC with a diameter of 10 nm, the effect of phonon confinement is significant. The peak shifted and broadened relative to the peak in bulk germanium (see Fig. 2). For sizes below 10 nm, the NCs Raman spectrum becomes asymmetric. The spectrum of the germanium NC with a diameter

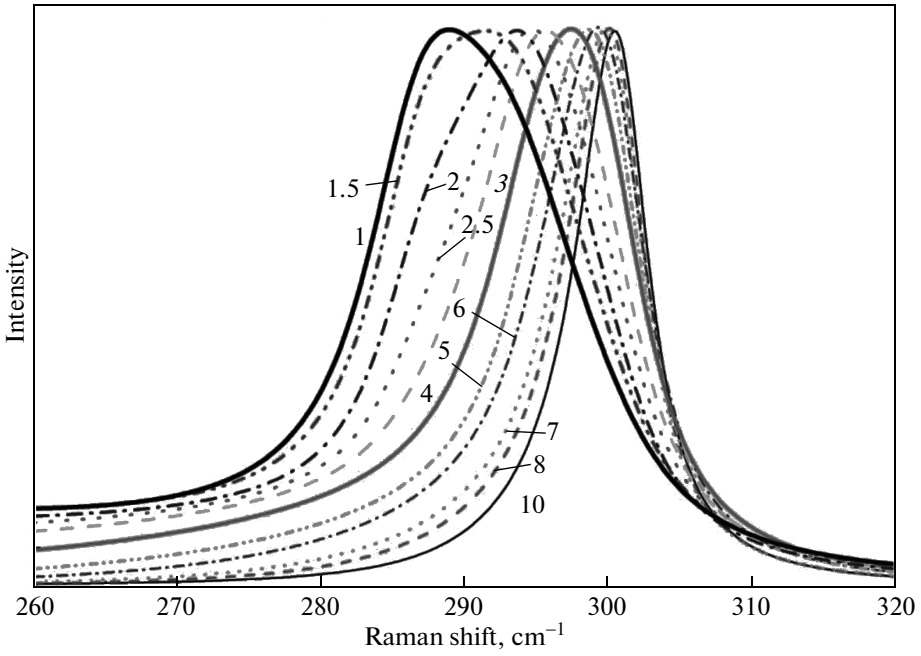

Fig. 3. Normalized calculated Raman spectra of Ge NCs with different diameters (from 10 to 1 nm, as indicated by numbers near the curves). The spectra are calculated using the improved PCM

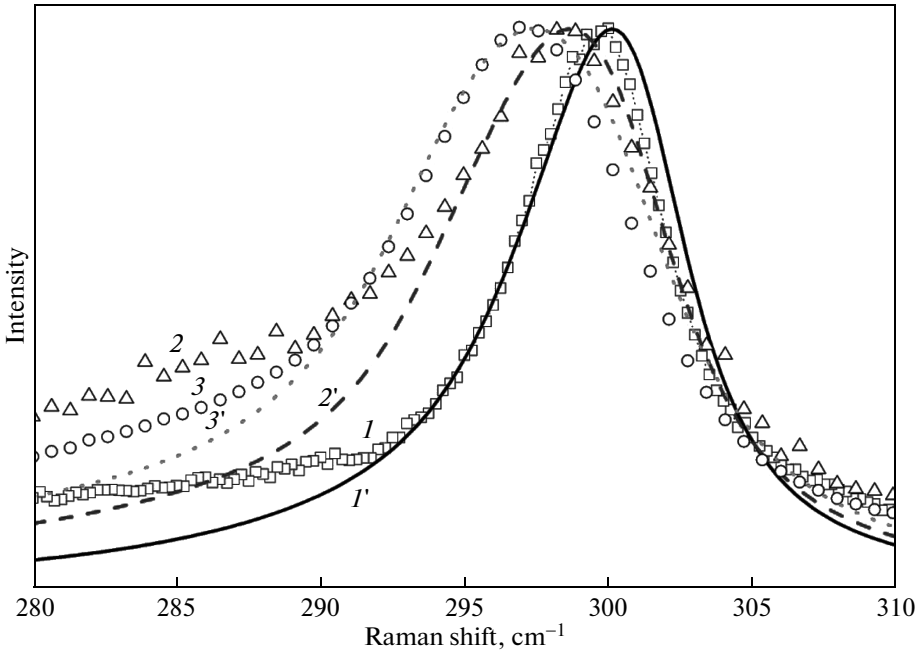

Fig. 4. Experimental (figures) and calculated (lines) Raman spectra of Ge NCs with different diameters: 7.5 nm (*1*, *1′*), 5.0 nm (*2*, *2′*), and 4.0 nm (*3*, *3′*). The spectra were calculated using the improved PCM

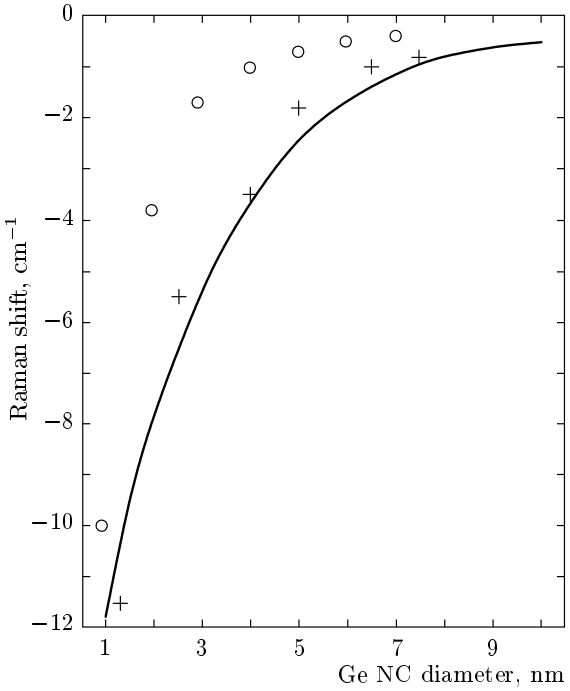

Fig. 5. Shift of the position of the Raman peak for optical phonons confined in Ge NCs of various sizes is shown relative to the position of the Raman peak for bulk Ge. Circles correspond to the data calculated in [23]; the solid curve corresponds to our results obtained using the improved PCM (dispersion is calculated in the Keating model taking the angular phonon dispersion into account); crosses show the experimental data

of 1 nm is different from the Raman spectrum of amorphous germanium, which is characterized by a broad band with a maximum at 275–280 cm^{-1}.

Figure 4 shows the normalized calculated Raman spectra and experimental Raman spectra of the samples. The average sizes of Ge NCs for these samples were determined from high-resolution transmission electron microscopy (HRTEM) data [19]. The operating voltage was 200 kV, the Si substrate was etched, and the films were thinned by Ar^+ ion milling [19]. The equipment of the "Nanostructures" Center, SB RAS, was used. The experimental spectra from Ge NCs with the sizes 7.5 and 4 nm (according to HRTEM data [19]) were obtained for samples grown with the use of the first method at the respective temperatures 580 and 500 °C. The experimental spectrum from Ge NCs 5 nm in size was obtained for the sample grown with the use of the second method (sample GeO_x(4 nm)/SiO_2(4 nm), annealed at 600 °C). In spite of the high-temperature annealing, the NC size was limited by the thickness of GeO_x layers. The position,

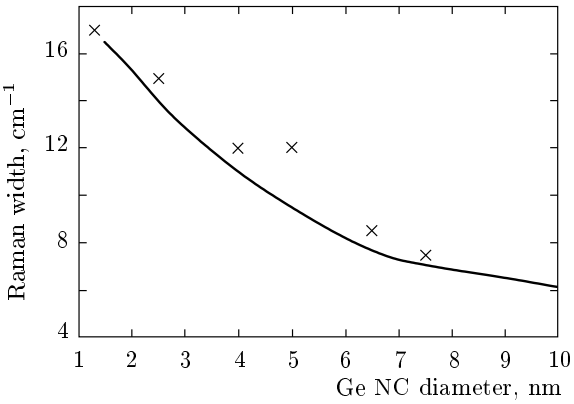

Fig. 6. Width of the Raman peak for optical phonons confined in Ge NCs of various sizes. The curve represents the results of calculation; crosses show the experimental data

shape, and width of the calculated and experimental peaks coincide well. Hence, the use of phonon angular dispersion calculated according to the Keating model allows describing the experiment very accurately.

Figures 5 and 6 summarize the results of calculations compared with experimental results. Figure 5 shows the difference between the position of Raman peaks of Ge NCs and bulk germanium. As mentioned above, the average sizes of the Ge NCs were determined from HRTEM data [19]. All samples were grown using the first and second methods, excluding the sample with the smallest Ge NCs. This sample is a sub-stoicheometric germanium oxide containing Ge NCs [15, 19]. As can be seen, the results of calculations in the improved PCM agree well with experimental data, but differ from the simulation results presented in [23]. We note that the results of calculations in the improved PCM are correct for a broad range of Ge NCs sizes (from about 1.3 to 10 nm). However, if the heating of the sample under the laser spot occurs during measurements, then the Raman peak experiences a shift (due to the anharmonicity of phonons). If the system contains mechanical stress, it also causes a shift of the Raman peak [17]. Figure 6 shows the dependence of the Raman peak width on the size of the NCs, for a calculation with the improved PCM and for experimental data. Some differences between the experimental data and the calculations are visible. In particular, the large width of the experimental spectra compared with the calculated spectra may be due to the dispersion of the size of the Ge NCs. If the anharmonicity effect due to heating or mechanical stress is not relevant, the present improved model allows determining the average size of the Ge NCs from the analysis of the Raman spectra for a wide range of sizes.

4. CONCLUSIONS

It is demonstrated that taking the angular dispersion of the TO and LO phonons into account and using the phonon dispersion curve described by the Keating model, it is possible to accurately determine the size of the Ge NCs from the analysis of their Raman spectra. The developed model correctly describes the experimental data for a wide range of Ge NCs sizes.

The authors are grateful to A. G. Cherkov (ISP SB RAS) for HRTEM studies of Ge NCs. One of the authors (V. A. V.) is thankful to the administration of Université de Lorraine for visit grants in 2012 and 2013. The authors are also thankful to the directorate of Scientific and Educational Center "Nanosystems and Advanced Materials", Novosibirsk State University for the possibilities to use the analytical equipment of the Center. This work was funded in part by the Presidium of the Russian Academy of Sciences (project № 24.29).

REFERENCES

1. A. I. Ekimov and A. A. Onushchenko, Pis'ma v Zh. Eksp. Teor. Fiz. **34**, 363 (1981).
2. S. Furukawa and T. Miyasato, Phys. Rev. B **38**, 5726 (1988).
3. I. Sychugov, R. Juhasz, J. Valenta, and J. Linnros, Phys. Rev. Lett. **94**, 087405 (2005).
4. H. Richter, Z. P. Wang, and L. Lay, Sol. St. Comm. **39**, 625 (1981).
5. I. H. Campbell and P. M. Fauchet, Sol. St. Comm. **58**, 739 (1986).
6. V. Paillard, P. Puech, M. A. Laguna et al., J. Appl. Phys. **86**, 1921 (1999).
7. G. Faraci, S. Gibilisco, P. Russo et al., Phys. Rev. B **73**, 033307 (2006).
8. P. Miska, M. Dossot, T. D. Nguen et al., J. Phys. Chem. C **114**, 17344 (2010).
9. I. F. Crowe, M. P. Halsall, O. Hulko et al., J. Appl. Phys. **109**, 083534 (2011).
10. G. Faraci, S. Gibilisco, A. R. Pennisi, and C. Faraci, J. Appl. Phys. **109**, 074311 (2011).
11. V. A. Volodin and V. A. Sachkov, Zh. Eksp. Teor. Fiz. **143**, 100 (2013).
12. M. Fujii, S. Hayashi, and K. Yamamoto, Appl. Phys. Lett. **57**, 2692 (1990).
13. X. L. Wu, T. Gao, X. M. Bao et al., J. Appl. Phys. **82**, 2704 (1997).
14. A. Wellner, V. Paillard, C. Bonafos et al., J. Appl. Phys. **94**, 5639 (2003).
15. E. B. Gorokhov, V. A. Volodin, D. V. Marin et al., Fiz. i Tekhn. Poluprovodnikov **39**, 1210 (2005).
16. I. D. Sharp, Q. Xu, D. O. Yi et al., J. Appl. Phys. **100**, 114317 (2006).
17. S. R. C. Pinto, A. G. Rolo, A. Chahboun et al., Thin Solid Films **518**, 5378 (2010).
18. J. E. Chang, P. H. Liao, C. Y. Chien et al., J. Phys. D **45**, 105303 (2012).
19. *Quantum Dots: Research, Technology and Applications* — Ge *Nanoclusters in* GeO_2 *Films: Synthesis, Structural Researches and Optical Properties*, ed. by R. W. Knoss, Nova Sci. Publ. Inc., New York (2008).
20. M. Ardyanian, H. Rinnert, X. Devaux, and M. Vergnat, Appl. Phys. Lett. **89**, 011902 (2006).
21. M. Ardyanian, H. Rinnert, and M. Vergnat, J. Appl. Phys. **100**, 113106 (2006).
22. V. A. Volodin, D. V. Marin, H. Rinnert, and M. Vergnat, J. Phys. D **46**, 275305 (2013).
23. Shang-Fen Ren and Wei Cheng, Phys. Rev. B **66**, 205328 (2002).
24. K. H. Khoo, A. T. Zayak, H. Kwak, and J. R. Chelikowsky, Phys. Rev. Lett. **105**, 115504 (2010).
25. P. N. Keating, Phys. Rev. **145**, 637 (1966).
26. G. Nelin and G. Nilsson, Phys. Rev. B **5**, 3151, **6**, 3777 (1972).